UC Santa Barbara

UC Santa Barbara Previously Published Works

Title

Mechanisms of contaminant transport in a multi-basin lake.

Permalink

https://escholarship.org/uc/item/8d32j5nr

Journal

Ecological applications : a publication of the Ecological Society of America, 18(8 Suppl)

ISSN

1051-0761

Authors

Rueda, Francisco J
Schladow, S Geoffrey
Clark, Jordan F

Publication Date

2008-12-01

DOI

10.1890/06-1617.1

Peer reviewed

eScholarship.org Powered by the California Digital Library
University of California

Ecological Applications, 18(8) Supplement, 2008, pp. A72–A87
© 2008 by the Ecological Society of America

MECHANISMS OF CONTAMINANT TRANSPORT IN A MULTI-BASIN LAKE

Francisco J. Rueda,[1,2] S. Geoffrey Schladow,[1,4] and Jordan F. Clark[3]

[1]*Department of Civil and Environmental Engineering, University of California, Davis, California 95616 USA*
[2]*Instituto del Agua—Universidad de Granada, 18071 Granada, Spain*
[3]*Department of Earth Science, University of California, Santa Barbara, California 93106 USA*

Abstract. Tracer studies are combined with a three-dimensional (3-D) numerical modeling study to provide a robust description of hydrodynamic and particle transport in Clear Lake, a multi-basin, polymictic lake in northern California, USA. The focus is on the mechanisms of transport of contaminants away from the vicinity of the Sulphur Bank Mercury Mine and out of the Oaks Arm to the rest of the lake and the hydraulic connection existing among the sub-basins of the lake. Under stratified conditions, the rate of spreading of the tracer was found to be large. In less than a week the tracer spread from the eastern end of the Oaks Arm to the other basins. Under non-stratified conditions, the tracer spread more slowly and had a concentration that gradually diminished with distance from the injection location. The numerical results showed that the mechanisms accounting for these observed patterns occur in pulses, with maximum rates coinciding with the stratified periods. Stratification acts first to enhance the currents by inhibiting vertical momentum mixing and decoupling the surface currents from bottom friction. The diversity of the flow structures that results from the interaction of the wind and the density fields in the lake is responsible for the high dispersion rates. Contaminants originating in the Oaks Arm are shown to be transported into the Lower Arm following the surface currents and into the Upper Arm mainly through the bottom currents. It was also shown that, under stratified conditions, both the baroclinic (density driven) gradients and the wind forcing act jointly to exacerbate the interbasin exchange.

Key words: circulation; Clear Lake, California, USA; particle transport; Sulphur Bank Mercury Mine; sulfur hexafluoride; three-dimensional model; tracer.

Introduction

Data presented here represent one component of a larger ecosystem-level study that traces the origin, transport, pathways, and fate of mercury (Hg) from the ore body at an abandoned Hg mine through the abiotic (sediment and water) compartments to lower trophic level species (benthic invertebrates and plankton) and ultimately to higher trophic level species (e.g., fish, birds, and mammals). This paper addresses the movement of dissolved components and particulates within Clear Lake in California, USA, by combining data from limnological tracer studies and 3-D numerical modeling that can elucidate the transport of Hg-contaminated particles from the Sulphur Bank Mercury Mine site throughout the rest of the Clear Lake aquatic ecosystem.

Understanding the transport pathways of dissolved species and suspended particles is of great interest in the management of lakes and reservoirs, especially at contaminated sites. Contaminant exposure, for example, may be difficult to determine in large and complex systems in which spatial heterogeneity is likely to occur (Knauer et al. 2000). Factors in determining potential exposure include proximity to sources, local aquatic chemistry, physico-biochemical reaction rates, the light environment, and the hydrodynamic processes of transport and mixing. The latter are key elements in understanding and predicting the spatial variability of contaminants, since they not only control the motion and dilution of particulate and dissolved species from the sources, but help determine environmental conditions that impact the biochemistry. Readers unfamiliar with hydrodynamic processes may find general texts (for example, Ramaswami et al. 2005) helpful in better understanding some of the material presented.

Tracer methods have long been used to address questions of transport and mixing, in part because of their relative simplicity and the graphical nature of their results. While effective in quantifying dispersion over long periods of time under one set of hydrodynamic conditions, they often yield insufficient temporal resolution to unambiguously describe the mechanisms of transport and dispersion. In large systems in which the tracer measurement grid is by necessity coarse, spatial resolution can also be an issue.

Manuscript received 26 September 2006; revised 9 July 2007; accepted 30 July 2007; final version received 16 September 2007. Corresponding Editor (ad hoc): B. Henry. For reprints of this Special Issue, see footnote 1, p. A1.

[4] Present address: Tahoe Environmental Research Center, University of California, Davis, California 95616 USA. E-mail: gschladow@ucdavis.edu

The present contribution seeks to combine tracer studies with a 3-D numerical model to create a more robust description of hydrodynamic and particle transport. With this approach it is shown how the tracer studies can be used to validate the model results, which provides the framework for greater insights into the precise mechanisms of transport. This approach will be applied to a particularly complex lake, Clear Lake, a multi-basin, polymictic lake in northern California. The hydrodynamics of Clear Lake have previously been described using field measurement (Rueda et al. 2003) and numerical modeling (Rueda and Schladow 2003) approaches. The numerical model was calibrated against an extensive set of temperature and velocity records collected in 1999 from one of the three basins of Clear Lake, the Oaks Arm. However, the effect of the complex hydrodynamic interactions on transport was not considered. This issue is particularly important to Clear Lake, one of the most Hg-contaminated lakes in the world (Suchanek et al. 1998, 2008). The main point source of Hg into the aquatic system, the Sulphur Bank Mercury Mine, is located on the shoreline of the Oaks Arm (Fig. 1). In the present paper we focus on the mechanisms of transport of contaminants away from the vicinity of the mine and out of the Oaks Arm to the rest of the lake and analyze in detail the hydraulic connection existing among the sub-basins of the lake.

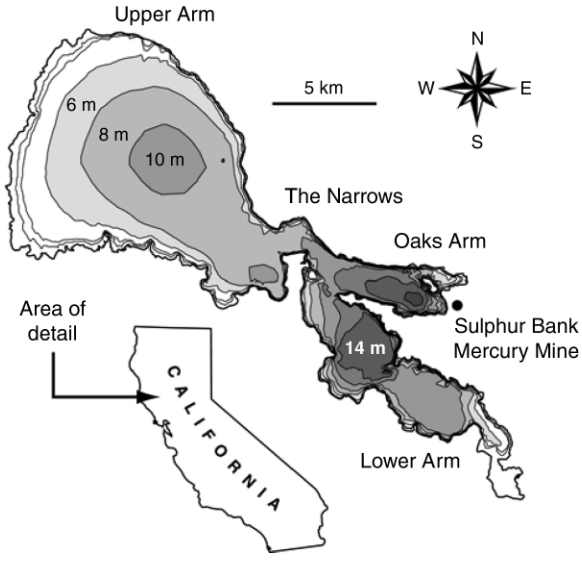

FIG. 1. A bathymetric map (in gray) of Clear Lake, California, USA, with contours shown every 2 m and the location of the Sulphur Bank Mercury Mine at the eastern end of the Oaks Arm.

Clear Lake and the Sulphur Bank Mercury Mine

Clear Lake is a large (176-km^2) eutrophic natural lake located 404 m above sea level (39°06′ N, 122°50′ W). The system is warm, relatively shallow (mean depth 8 m), and polymictic. It is naturally divided into three distinct sub-basins or arms: the Upper Arm, the Lower Arm, and the Oaks Arm (Fig. 1). The large shallow basin of the Upper Arm comprises 72% of the lake's surface area and receives >90% of the watershed runoff. A narrow passage (the Narrows) connects the Upper Arm with the two other arms of the lake, both of which are considerably narrower and deeper than the Upper Arm. The Lower Arm is a conduit to the lake's only outlet, Cache Creek, at the extreme southeast end of the lake. With a mean residence time of two to three years, advective flow through the lake is not a major factor in water movement (Lynch 1996). Rather, water movement in Clear Lake is mainly the result of a subtle interaction between the wind field and stratification, modulated by the Earth's rotation (Rueda and Schladow 2003, Rueda et al. 2003).

At the eastern end of the Oaks Arm is the Sulphur Bank Mercury Mine, the main source of Hg to Clear Lake (Suchanek et al. 2008). The mine site, which is presently abandoned, contains a large water-filled pit filled with pH 3 fluids, the Herman Pit, and large quantities of mine tailings and waste rock (Suchanek et al. 2008). From 1873 to 1957 mining operations removed between 4400 and 7000 Mg of Hg from the site and resulted in ~100 Mg of Hg being deposited into the aquatic ecosystem of Clear Lake (Chamberlin et al. 1990). Two major sources of Hg have been identified in the Clear Lake system (Suchanek et al. 2008). First, inorganic Hg from the erosion of Hg-contaminated waste rock and tailings piles has contaminated Clear Lake for many decades. Drainage and slope stabilization at the mine site by the U.S. Environmental Protection Agency (U.S. EPA) in recent years have probably reduced this source. Second, acid mine drainage containing dissolved Hg enters the lake in near-shore areas of the mine as well as through preferred conduits and groundwater seepage to sub-sediment pathways out into Clear Lake. Methylmercury (a highly toxic and readily bioavailable form of Hg) is produced as a metabolic by-product of bacterial activity on inorganic Hg within the lake's sediment and on flocculent material (floc) formed adjacent to the mine site as a result of acid mine drainage into the lake. Tracer release studies indicate that water could be seeping from Herman Pit into the lake at rates as high as 630 L/s (Oton et al. 1998, Schladow and Clark 2008). Once formed, the floc becomes transformed over several months to a medium rich in methyl Hg, which in turn is prone to resuspension and could easily be transported by currents. Concern over the transport of this flocculent material has motivated the present work.

The internal circulation of the Oaks Arm: a review

During times when the Oaks Arm is vertically stratified in temperature, circulation is characterized by a marked diurnal periodicity dominated by the wind regime. Typically, winds out of the northwest develop during the afternoon and evening hours. In response to the wind, near-surface and warmer water moves toward

the east, accumulating in the downwind end of the basin, while colder and deeper waters are displaced to the west, accumulating near the upwind end of the basin. As a consequence, horizontal temperature gradients are generated in this weakly stratified system both along the longitudinal axis of the Oaks Arm and also across the system, due to rotational effects. During the night and early morning hours, when the wind ceases, the baroclinic pressure gradients that result from the horizontal differences in temperature become the dominant forcing mechanism in the system, driving currents of up to 10–15 cm/s westward at the surface and eastward near the bottom (Rueda and Schladow 2003, Rueda et al. 2003).

The daily setup and relaxation of the temperature gradient is modulated by the influence of the earth's rotation, creating a residual circulation referred to as wind baroclinic pumping (Rueda et al. 2003). The cyclonic residual circulation that results is superimposed on the direct wind-driven circulation, also of cyclonic nature, enhancing the rates of transport. Rueda and Schladow (2003) showed that the change of circulation patterns from wind-driven to density-driven (baroclinic) does not occur simultaneously throughout the Oaks Arm. On the contrary, the change in circulation has the character of a wave, starting at the downwind end of the arm and proceeding westwards. The rate of longitudinal propagation of such a wave differs along the north and south shores of the Oaks Arm, being faster along the north shore. Consequently there are locations on the south of the Oaks Arm where the baroclinic circulation rarely replaces the wind-driven circulation, while on the north shore the baroclinic circulation is felt more frequently and more intensely. This difference in the amount of time the baroclinicly driven vertical circulation dominates the wind-driven motions on the north and the south sides of the basin is reflected in the cyclonic nature of the residual circulation: westward flow in the north, eastward flow in the south. This cyclonic circulation was noticeably revealed by the trajectories of several autonomously recording drogues deployed in 1999 (Rueda et al. 2003).

Methods

Tracer experiments

Three tracer experiments were performed to resolve the fate of water masses from the Oaks Arm at times of different stratification intensity. The first two experiments, in August and November 1995, used the fluorescent tracer Rhodamine-WT (Abbey Dye, Philadelphia, Pennsylvania, USA). The third experiment, in August 1997, used sulfur hexafluoride (SF_6) as a tracer. Sulfur hexafluoride has been used as a deliberate tracer in continental aquatic systems for more than a decade (e.g., Wanninkhof et al. 1985, 1987, Clark et al. 1994, 1996, 2004, Gamlin et al. 2001). Sulfur hexafluoride differs from ionic tracers in that it is a low-solubility gas and is lost from the system at the air–water interface. Because we were interested in the transport of potential contaminants emanating from the mine, the initial release point for all the tracer experiments was in the southeast portion of the Oaks Arm. For the two August experiments, the water column was thermally stratified, ranging from ~28°C at the surface to 23°C near the bottom. For the November experiment the lake was essentially homogenous at ~16°C.

Experiments I and II: Rhodamine-WT

Rhodamine-WT solution was diluted with lake water prior to injection to minimize density differences with the ambient lake water. Injection occurred through a 0.6 m long perforated diffuser to further enhance dilution to ~10 ppb. Both experiments released the tracer at the surface, and the injections took place in the late morning. In the 23 August tracer injection, 21 kg of 20% stock solution was used. In the 9 November tracer injection, 52 kg of 20% stock solution was used. Tracer concentration was measured in situ using a Turner Model 10-AU-005 fluorometer (Turner Designs, Sunnyvale, California, USA), with a limit of detectability of 0.005 ppb. Water was drawn through the fluorometer from an intake hose that could be lowered to any depth in the lake. Sufficient time was allowed for the hose to flush between successive readings. Sampling continued for three days after the injection. For both experiments the wind was generally from the northwest and peaked each day at ~6 m/s in the Oaks Arm (Lynch 1996).

Experiment III: sulfur hexafluoride

Approximately 0.9 moles (130 g) of SF_6 were injected into the Oaks Arm of Clear Lake during the morning of 5 August 1997. The gas was injected by bubbling through a diffusion stone submerged to a depth of ~10 m. An unknown fraction of the gas dissolved during its transit through the water column; the remainder escaped to the atmosphere. The wind speed for the few days after the injection was from the northwest and peaked in the early evenings at ~5 m/s.

Water samples were collected 5 h, 1 d, 2 d, 12 d, and 20 d after the injection. During each sampling event, water was collected into biological oxygen demand (BOD) bottles using a submersible pump along a predetermined grid pattern. Care was taken not to entrain any air into the bottles or to leave any headspace. At each station samples were collected 1 m below the surface, at mid-depth (only at stations deeper than 10 m), and 1 m above the sediments. At a field laboratory, a known volume of water (~35 mL) was transferred from the BOD bottles into 50-mL glass syringes. After adding a known volume (~15 mL) of ultra-high purity nitrogen gas, the syringes were shaken for 3 min. The headspace gas was then analyzed on a gas chromatograph equipped with an electron capture detector (Wanninkhof et al. 1987). With this method, the detection limit was 0.05 pmol/L and the analytical uncertainty was ±3%. It is important to note that the detection link is greater than the Henry's Law

equilibrium value (<0.002 pmol/L) with the modern atmosphere (Busenberg and Plummer 2000, Bullister et al. 2006).

The numerical tools

The 3-D hydrodynamic and transport model.—Currents in Clear Lake were simulated using a 3-D free surface hydrodynamic model, SI3D-L. The model is based on the continuity equation for incompressible fluids, the Reynolds-averaged form of the Navier-Stokes equations for momentum, the transport equation for temperature, and an equation of state relating temperature to fluid density. The governing hydrodynamic equations are solved in layer-averaged form using a semi-implicit, three-level, leapfrog-trapezoidal finite difference scheme on a staggered Cartesian grid (Smith 1997). The transport equation for temperature is solved using a two-level semi-implicit scheme that uses operator splitting. Only the vertical diffusion in the governing equation is treated implicitly, using a trapezoidal method. The 1-D advection operators in each of the three Cartesian directions are discretized with flux-limiter methods. The corrected fluxes are constructed with the monotone upstream differencing scheme, the Lax-Wendroff second-order method, and the Van Leer MC limiter. Turbulent mixing is represented in the 3-D model using diffusion-like terms based on the level 2.5 Mellor-Yamada turbulence model (Kantha and Clayson 1994). Further details on the numerical methods can be found in Smith (1997), Rueda (2001), and Rueda and Schladow (2002).

The 3-D model was run for a period from 20 to 28 May 1999 (simulation period), during which the lake was thermally stratified, with vertical temperature differences as high as 4.2°C. It is only during that period of time (and not during the three periods when the tracer field experiments took place), when sufficient data exists to prescribe the initial conditions and dynamic forcing. Hence, a direct comparison cannot be made between the results of the numerical model and the field tracer experiments. Nevertheless, and because both approaches yield information about the flow and transport, comparisons of the different time periods are still highly instructive.

The domain of Clear Lake was discretized by constructing a grid with 100-m resolution in the horizontal direction and 1-m resolution in the vertical direction. The model time step was 180 s. A description of the field data used for validation and the forcing conditions, in particular the highly resolved wind field, is presented in Rueda et al. (2003, 2005). The veracity of the model in representing the details of the flow field at Clear Lake is also demonstrated in Rueda and Schladow (2003). Once validated, the three-dimensional velocity field calculated with the hydrodynamic model was used to analyze, using a Lagrangian particle-tracking model and an Eulerian tracer transport model, the migration paths of particles and tracers released in arbitrary locations within the aquatic system. The tracer transport model is built with the same algorithms existing in SI3D-L for temperature and other active scalars.

Lagrangian particle-tracking model.—In the particle-tracking model the particle position is given by the summation of successive infinitesimal displacements over time. The infinitesimal displacements are described by the equation

$$dx_i = \underset{\text{(term 1)}}{a_i\,(\mathbf{x},t)} \times dt + \sum_{j=1}^{3} \underset{\text{(term 2)}}{b_{ij}\,(\mathbf{x},t)} \times dW_j(t) \qquad (1)$$

where the right hand side consists of a deterministic part (term 1) and a stochastic part (term 2). The coefficients a_i and b_{ij} satisfy the following equations (Dunsbergen and Stelling 1993):

$$a_i = u_i + \sum_{j=1}^{3} \frac{\partial D_{ij}}{\partial x_j} \qquad (2)$$

$$\frac{1}{2}\sum_{k=1}^{3} b_{ik} b_{jk} = D_{ij}. \qquad (3)$$

Here x_i and u_i are the particle position and velocity, D_{ij} is the diffusion tensor in the flow field, and $W_j(t)$ is a Wiener or Brownian motion process. The simulated velocity field is interpolated to the particle position using the method proposed by Pollock (1988). The eddy diffusivity D_{ij} in the model varies linearly with vertical direction between two consecutive nodes in a grid column, and it is assumed constant in the horizontal directions (Rueda 2001). With those assumptions the diffusion tensor becomes diagonal and considerable simplification is obtained in the implementation of this method. The deterministic part represents the advective transport and also includes the influence of the gradient of turbulent diffusivity, needed for consistency with the advection-diffusion equation (see Dimou and Adams 1993, Kitanidis 1994). Output of the hydrodynamic model at 30-min intervals was interpolated to provide velocity fields at 5-min intervals. The stochastic displacement mimics the effects of turbulent processes in the particle trajectory. The discretized version of Eq. 1 that represents the transition from the state (or particle position) at $n\Delta t$ to the state at $(n+1)\Delta t$ is given as

$$x_i^{(n+1)} = x_i^{(n)} + a_i(\mathbf{x}^{(n)}, n\Delta t) \times \Delta t + \sum_{j=1}^{3} b_{ij}(\mathbf{x}^{(n)}, n\Delta t) \times \Delta W_j(n\Delta t) \qquad (4)$$

where the bold variables are vector quantities. The factor $\Delta W_j(t)$ is simulated by a Gaussian number generator, with $E(\Delta W_j) = 0$ and $E(\Delta W_i \Delta W_j) = \delta_{ij}\Delta t$.

Results and Discussion

Tracer field experiments

Experiment I with Rhodamine-WT under stratified conditions (August).—The tracer was visually present at

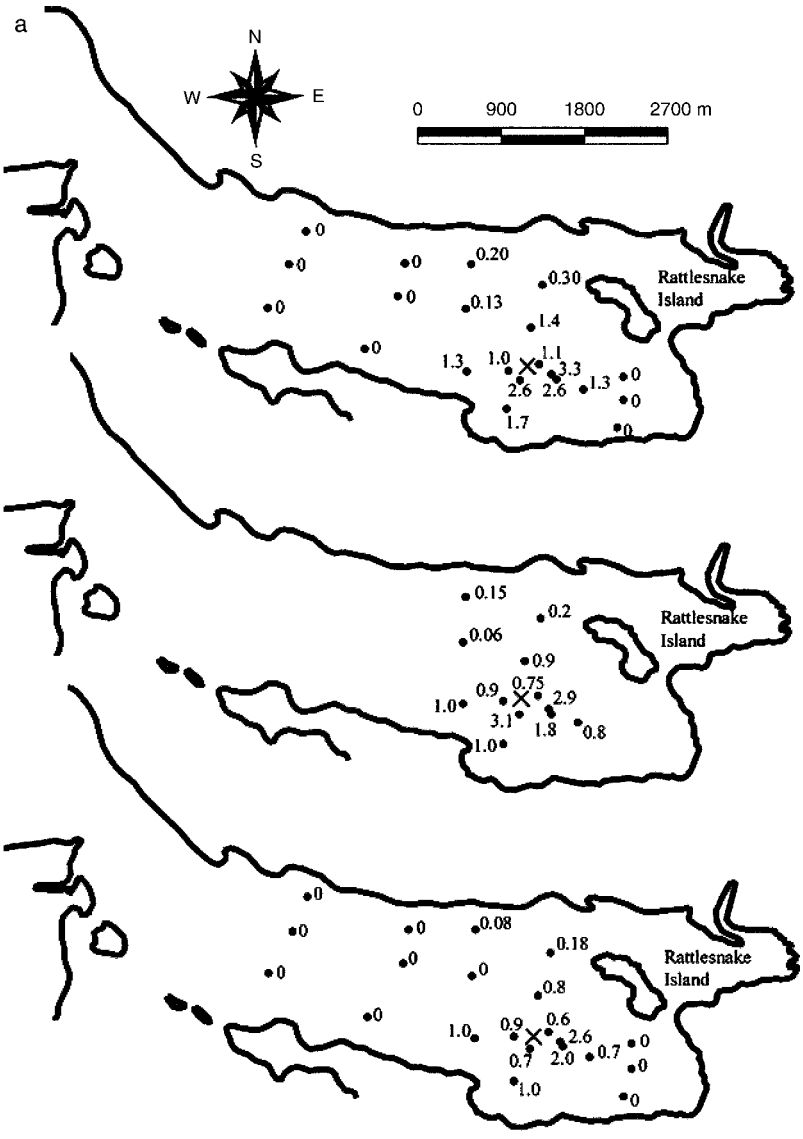

FIG. 2. Concentrations (ppb) of Rhodamine-WT at the surface (top panels), 5 m below the free surface (middle panels), and bottom of the lake (bottom panels) as measured in experiment II on (a) 9, (b) 10, and (c) 11 November 1995. The × denotes the injection location.

the surface immediately after the injection. The first measurements were taken at the injection site ~3 h after finishing the tracer injection. No Rhodamine-WT was detected, and sampling throughout the lake over the succeeding three days also failed to detect Rhodamine-WT. This is attributed to advection producing rapid transport of the dye away from the injection site, and the sample boat subsequently being in the wrong place at the wrong time. Sampling was initially to the east of the injection site, in expectation of the tracer to move in the direction of the wind. However, subsequent analysis of acoustic Doppler current profiler (ADCP) measurements and numerical simulations (Rueda and Schladow 2003, Rueda et al. 2003) suggest the existence of a flow convergence causing the tracer patch to downwell and to be advected westward at depth along the northern side of the Oaks Arm. Other explanations of the "disappearance" were explored, including incorrect standardization of the fluorometer and uptake or modification of the Rhodamine-WT by algae. However, all these possibilities were eventually ruled out.

Experiment II with Rhodamine-WT under non-stratified conditions (November).—Tracer concentration profiles were collected at 54 stations over the three-day sample period. Plots of the surface, 5 m, and bottom concentrations 1 m above the sediment are shown in Fig. 2. By the end of the first day (Fig. 2a), the patch's center had moved east of the injection site and had dispersed over a distance of ~1.5 km to the north and south. The similarity of top and bottom measurements indicates

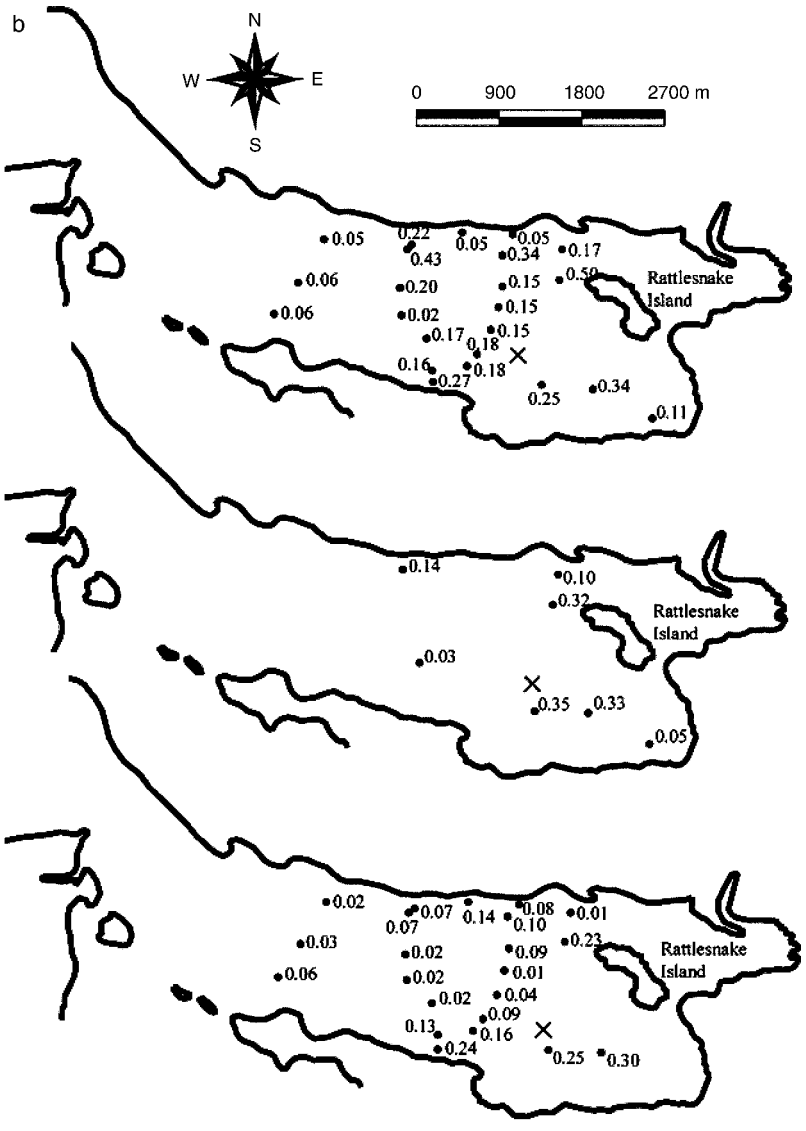

FIG. 2. Continued.

rapid vertical mixing during this period. In the afternoon of 10 November (Fig. 2b), tracer was found near the north and south shores and in the vicinity of the mine. The ratio of bottom concentration to surface concentration decreased with distance from the injection point, suggesting the tracer near the bottom was dispersing at a slower rate than that in the surface water. Rhodamine-WT was still detectable on the last day of the study and distributed fairly evenly throughout the eastern two-thirds of the Oaks Arm (Fig. 2c). Spot measurements failed to find any detectable tracer outside the Oaks Arm.

Over the three days, the dye patch retained a diffusion-dominated appearance, with the highest concentrations closest to the injection point and concentration typically decreasing with distance. An overall diffusivity was estimated following Fischer et al. (1979) and yielded a diffusivity coefficient on the order of 10 m^2/s. This diffusivity is larger than values calculated for a small, sheltered lake, 0.005–0.025 m^2/s (Lawrence et al. 1995) and more similar to those for coastal waters, which are typically 0.2–30 m^2/s (List et al. 1990).

Experiment III with sulfur hexafluoride under stratified conditions (August).—Sulfur hexafluoride concentrations in samples collected prior to the injection were below the limit of detection. Five hours after the injections, tracer was found at only one station within 300 m of the injection point. The patch grew substantially thereafter. One day after the injection, SF_6 was detected in all surface samples collected from the 15 km long Oaks Arm. The highest concentrations were found to the south of the injection point and along the

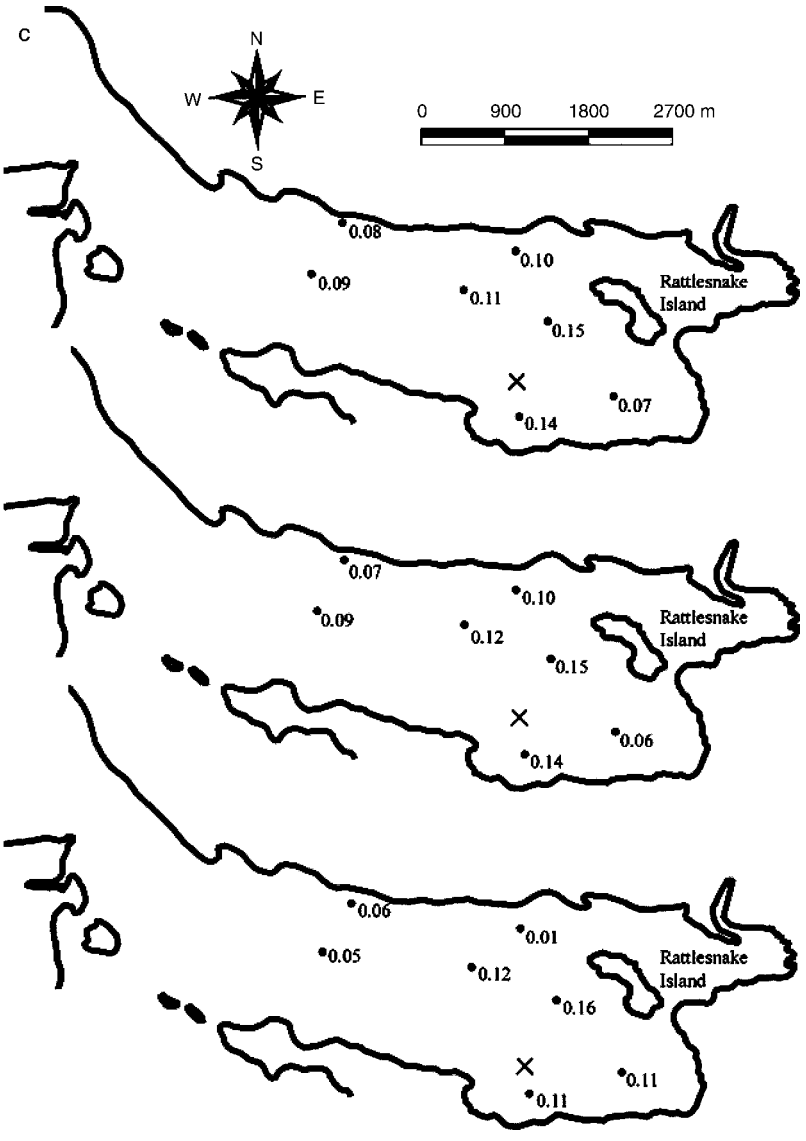

FIG. 2. Continued.

northern shore. In bottom samples, SF_6 was detected only in few stations near the injection point. Clearly, during this stratified period, transport within the surface layer was much stronger than in the bottom layer and the two layers were acting independently. The distribution of tracer on day 2 was very similar to day 1 (Fig. 3), with the exception that in the surface water the tracer was beginning to move from the Oaks Arm into the Lower Arm and in bottom water, the tracer had spread slightly more to the north.

Fourteen days after the injection, tracer was found throughout all basins at both the surface and the bottom (Fig. 4). The data displayed significant patchiness. The concentration was the highest from stations located in the Oaks Arm. Outside the Oaks Arm, the highest value was at the bottom of the Upper Arm. Seven days later, the distribution had not changed significantly, although the maximum observed concentrations in the Oaks Arm had diminished by 20%, and those values were similar to the peak values in both the Upper and Lower Arms. This is consistent with the lake becoming homogeneous and the loss of tracer due to gas exchange.

Numerical experiments

Effects of temperature stratification on horizontal transport.—

1. *Particle release experiments in 3-D.*—Model outputs of the velocity at 30-min intervals, during the simulated period, were interpolated in time to yield 5-min velocity fields. The interpolated fields were then

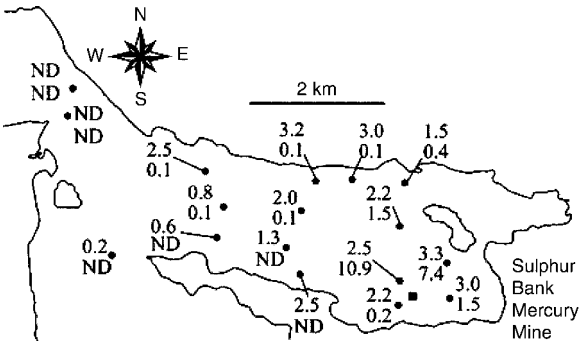

FIG. 3. Distribution of sulfur hexafluoride in the Oaks Arm on 7 August 1997, two days after the injection. The pairs of numbers indicate the concentration (pmol/L) in the surface (1 m, top number) and bottom (>10 m, bottom number) water. The solid square denotes the location of the tracer injection. The abbreviation "ND" indicates that the tracer was not detected (<0.05 pmol/L).

used to simulate the transport of a total of 100 particles released at 01:00 on day 139 (20 May) at the horizontal locations shown in Fig. 5a, assigned using a Gaussian distribution with a standard deviation of 400 m. The locations of the particles in the vertical were randomly assigned again using a Gaussian distribution centered at 1.5 m with a standard deviation of 1.5 m. The particles were simply carried by the currents, and no random displacements were added to simulate the effects of turbulence (although the momentum equation solved includes the effects of turbulence).

Fig. 5b shows the locations of the particles 8 d after their release. Some of them had migrated to the Upper and Lower Arms, almost 12–14 km from their original location. The mean path length followed by the particles during the 8-d period was ~21 km. This apparent dominance by advection under stratified conditions is consistent with the observations in tracer experiments I and III.

The simulated particle trajectories are also consistent with the hydrodynamic description of Clear Lake. To describe the particles' 3-D trajectories, plan-view (2-D) plots have been used. In these plots, the depth below the surface of the particle is indicated by the grayscale of the position marker. The positions are shown every hour, so an increased spacing between positions indicates higher velocities. Fig. 6a shows the trajectory of a particle that, after plunging and rising twice at the downwind end of the Oaks Arm, is carried on day 142 by surface currents to the westernmost end of the Oaks Arm and into the Lower Arm. The particle plunges following the wind-driven downwelling currents close to the mine (as is presumed to have occurred to the tracer patch in experiment I), and it rises to the surface at the embayment located at the southwest edge of the Oaks Arm. In the Lower Arm the particle trajectory describes several clockwise loops, offering a very illustrative example of the wind-driven direct negative vorticity circulation that exists in the Lower Arm (Rueda et al. 2003). The trajectory shown in Fig. 6b is that followed by a particle that, once it reaches the bottom, follows the westward currents of the lower layers along the north shore of the Oaks Arm to end up 8 d later in the Upper Arm. A third particle (Fig. 6c) describes counterclockwise loops within the Oaks Arm, illustrating the positive vorticity of the sub-basin circulation. The highly variable nature of this advectively dominated flow is consistent with the results of the SF_6 tracer experiment.

Fig. 7a describes the trajectory of a particle affected by the baroclinicly driven return flow on day 144 that is confined to the north shore of the Oaks Arm. The particle covers ~2–3 km in 13 h from site 1 in the figure at 02:00 on day 144 to site 2 at 15:00 under calm conditions. Prior to this the particle is subject to the strong downwelling already noted at the east end of the Oaks Arm. The time series of the east–west velocity component of the particle is shown in Fig. 7b. It exhibits first a change in the direction of motion from eastward to westward in the late evening of day 144, and then it experiences consistent negative, i.e., westerly, values during the evening and early morning hours of that same

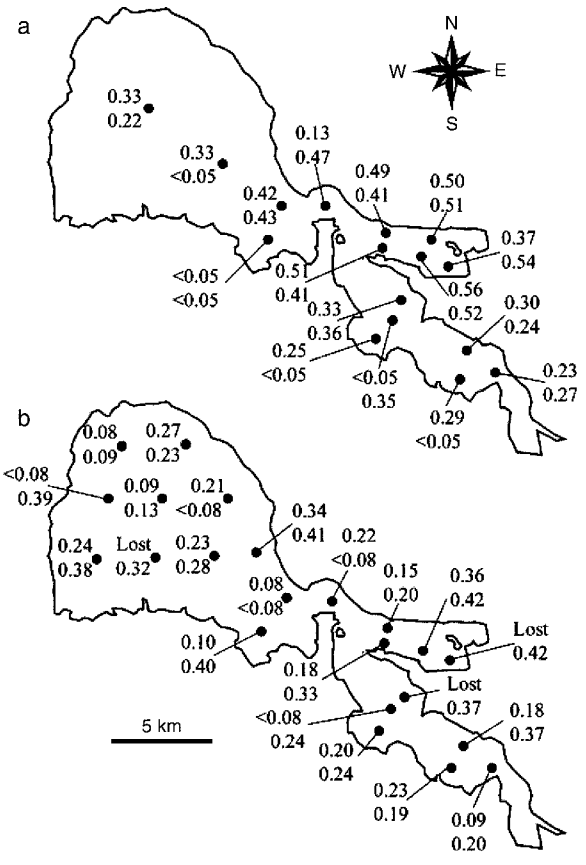

FIG. 4. Distribution of sulfur hexafluoride in Clear Lake on (a) 19 August and (b) 25 August 1997. The pairs of numbers indicate the concentration (pmol/L) in the surface (1 m, top number) and bottom (>10 m, bottom number) water.

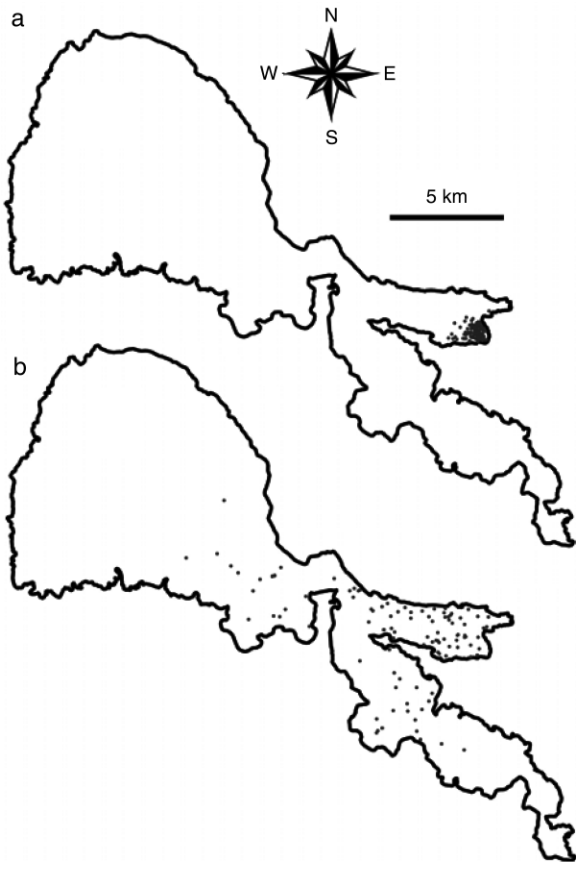

FIG. 5. Projection onto a horizontal plane of all simulated particles (a) 1 h after release and (b) 8 d after release.

day. Eventually the particle is transported to the Upper Arm.

The effect of stratification on horizontal transport was evaluated by modeling the transport in Clear Lake during the simulation period, using a modified version of the model in which the heat fluxes at the surface were reduced. The maximum temperature difference attained in the 8 d of simulation with the modified code, measured at the deepest point of the Oaks Arm (14–15 m deep), was 0.7°C. This experiment will be referred to as experiment NST (for non-stratifying), to differentiate it from the experiments in which realistic heat fluxes are used to drive the model. The latter will be referred to as experiment ST. In experiment ST, stratification develops as revealed by the observations (see Rueda and Schladow 2003). The velocity field simulated with the "modified" code was then used to run the same particle tracking exercise. Several aspects stand out. The mean transport rate of the 100 particles decreased considerably in this exercise in comparison to experiment ST. The mean path length of the particles was ~8 km, in contrast with the 21 km calculated for experiment ST. None of the 100 particles released in the vicinity of the mine in the Oaks Arm entered either of the other two arms (Fig. 8), and the overall spread is of a more diffusive nature, with maximum particle concentrations remaining in the vicinity of the release point, even after 8 d. Over the 8-d simulation period a weak circulation pattern was apparent in the Oaks Arm, taking the form of a wind-driven recirculation cell in a vertical plane that is oblique with respect to the longitudinal axis of the Arm, as illustrated by the particle trajectory shown in Fig. 9. The downwelling region is to the east and south in the Oaks Arm, and the upwelling region is at its northwest end. It should be noted that the wind forcing was identical in both experiments ST and NST.

2. *Dispersion statistics from particle tracks.*—The effect of stratification is not only to increase the rate of transport of particulate material by intensifying the

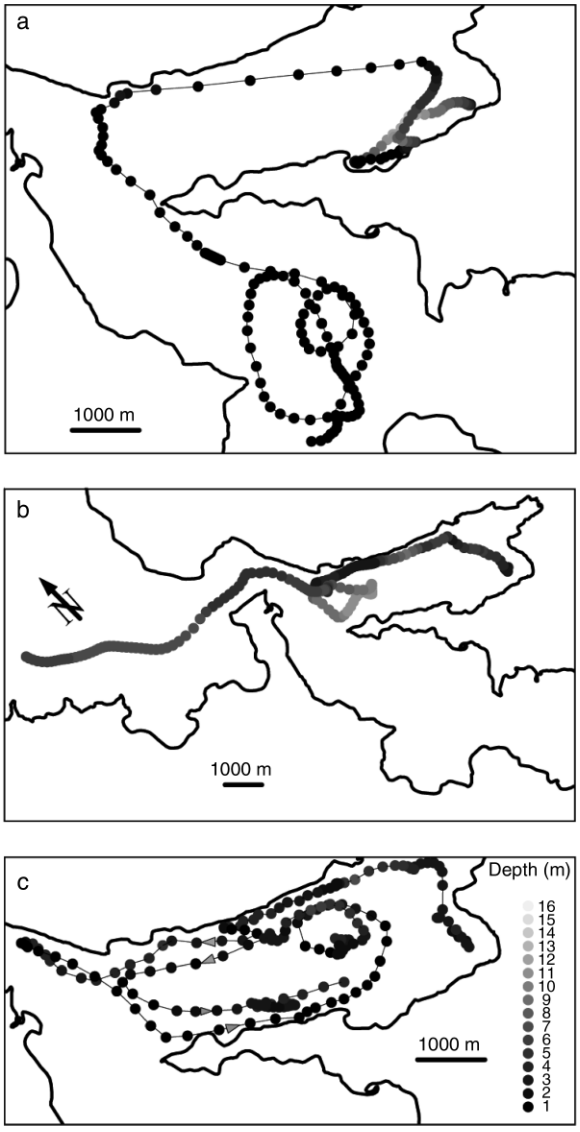

FIG. 6. Simulated trajectories followed by three selected particles. The arrows in panel (c) indicate the direction of the particle motion (westward in the north, eastward in the south). Symbols are plotted 1 h apart.

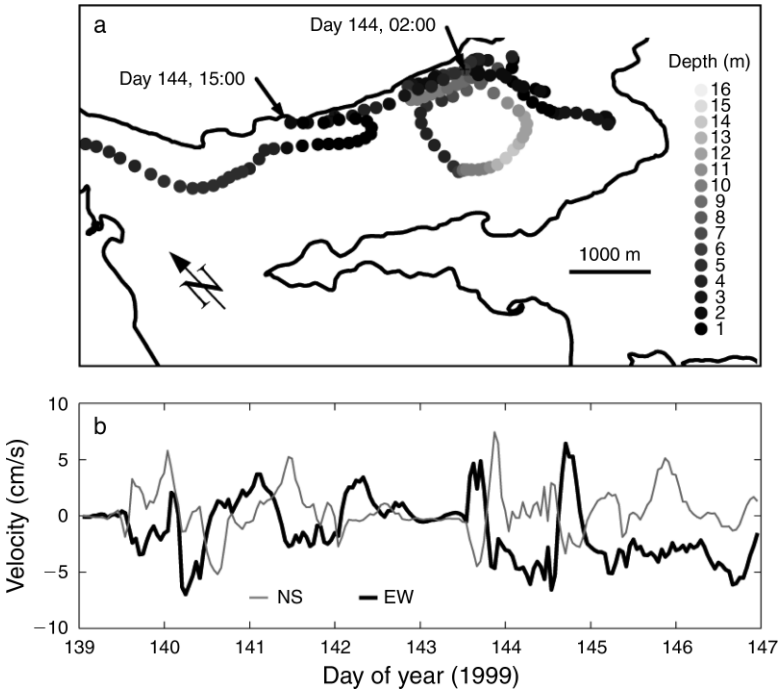

FIG. 7. (a) Simulated trajectory of a particle illustrating the effect of baroclinic forcing during calm periods. The locations of the particle at 02:00 on day 144 and 13 h later are indicated. (b) Time series of the simulated particle velocity.

currents but also to increase the rate of dispersion of such particles. First, it is well known that mixing of momentum is inhibited by stratification, and hence, the shear in the water column will increase during stratified periods, leading to increased dispersion rates. However, other mechanisms can also have a significant impact in the dispersion of particle clouds in large water bodies (Fischer et al. 1979:233). To separate the effects of vertical and horizontal processes on dispersion, particles were constrained to move in a horizontal plane only (as would a blind drogue in a real experiment). A patch of 100 such particles was released 2.5 m below the surface at 12:00 on day 143. The centroid of the particle cloud was initially located close to the mine site in the Oaks Arm, with a standard deviation about the centroid of 400 m. The particle-tracking experiment was conducted with the simulated velocity field under both stratified conditions (ST) and non-stratified conditions (NST). The diffusion tensor was set to zero in the vertical and equal to 1 m^2/s in both horizontal directions.

In experiment ST, the net displacement of the centroid of the particle cloud was ~7400 m, while in experiment NST it was only 1600 m, revealing again a more energetic velocity field during stratified conditions. The dispersion of the particle distribution, σ^2, was calculated from the variance of the particle positions in each horizontal coordinate direction (List et al. 1990) as

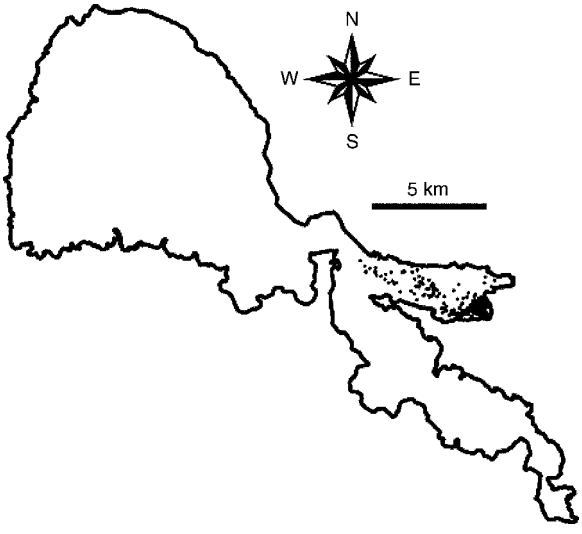

FIG. 8. Projection onto a horizontal plane of all simulated particles 8 d after release for the non-stratified case.

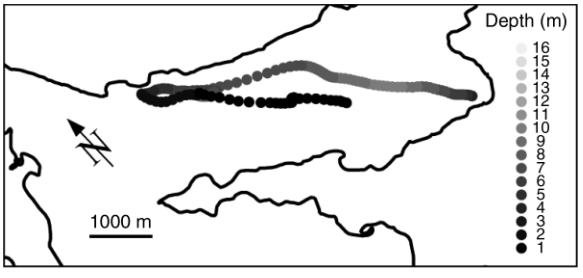

FIG. 9. Simulated trajectory followed by a selected particle for the non-stratified case.

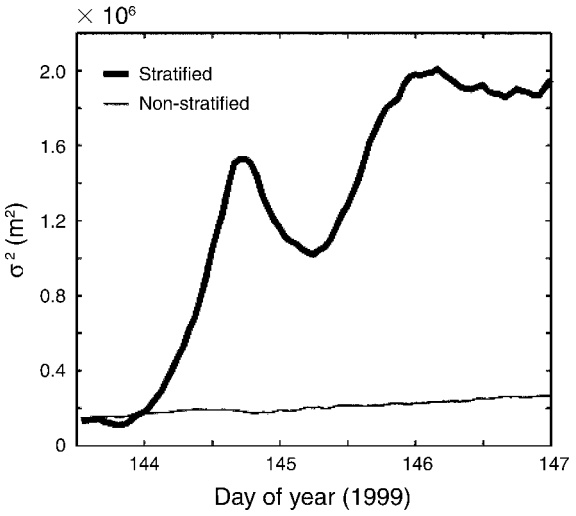

FIG. 10. Time series of simulated dispersion of the particle distribution, σ^2, under stratified and non-stratified conditions, as calculated by the numerical model.

$$\sigma^2 = \frac{1}{2}\left[\frac{1}{N}\sum_{i=1}^{N}(x_i - \mathbf{X})^2 + \frac{1}{N}\sum_{i=1}^{N}(y_i - \mathbf{Y})^2\right] \qquad (5)$$

where x_i and y_i represent horizontal location of particle i in the cloud at any given moment in time, and $\mathbf{X}$, $\mathbf{Y}$ represent the horizontal coordinate of the cloud's centroid at that same time. The evolution of σ^2 as a function of time t has been plotted in Fig. 10 for both experiments. The dispersion coefficient $K(t)$ is calculated as

$$K(t) \approx \frac{1}{2}\frac{\Delta\sigma_i^2}{\Delta t} \qquad (6)$$

and it reaches much higher values in experiment ST than in experiment NST. The maximum dispersion coefficient in the ST experiment is 20 m^2/s, while it is only 1.7 for the NST experiment. For NST, turbulent diffusion processes (parameterized by the diffusion tensor D_{ij} in Eq. 2) dominates the dispersion coefficient, as suggested by the similar order of magnitudes of $K(t)$ and D_{ij}. This is not the case for ST. The dispersion, in this case, does not increase monotonically with time, as it must if only diffusion were dominating dispersion. Rather, the dispersion rate undergoes diurnal oscillations, which are related to the baroclinic pumping mechanism of circulation. The Oaks Arm is at the downwind end for the typically northwesterly, diurnal winds acting on Clear Lake, which will cause the surface horizontal currents to converge in its eastern end (the mine site). The particles will tend to accumulate in the convergence areas and, thus, its dispersion will decrease in the Oaks Arm. Following the wind events, several mechanisms contribute to the increase in the dispersion rates. Those mechanisms include horizontal divergence γ, relative vorticity η, stretching α, and shearing deformation h, which are defined from the velocity field and for a given point 0 (see e.g., Halide and Sanderson 1993) as follows:

$$\gamma \equiv \left(\frac{\partial U}{\partial x}\right)_0 + \left(\frac{\partial V}{\partial y}\right)_0 \qquad (7)$$

$$\eta \equiv \left(\frac{\partial V}{\partial x}\right)_0 - \left(\frac{\partial U}{\partial y}\right)_0 \qquad (8)$$

$$\alpha \equiv \left(\frac{\partial U}{\partial x}\right)_0 - \left(\frac{\partial V}{\partial y}\right)_0 \qquad (9)$$

$$h \equiv \left(\frac{\partial V}{\partial x}\right)_0 + \left(\frac{\partial U}{\partial y}\right)_0. \qquad (10)$$

Here U and V denote the velocity of water in the east–west (positive toward the east) and north–south (positive toward the north) directions, respectively. The rate of stretching deformation, α, is the change of shape by different rates of stretching along the coordinate axes. If this deformation is positive, there is stretching along the x-axis and shrinking along the y-axis. The rate of shearing deformation is simply the difference between the two Cartesian components of stretching. Vorticity is defined as twice the angular velocity of water parcels, and divergence quantifies the rate at which a cloud of particles, initially close to each other, will expand or compress. We have followed here a simple methodology proposed by Okubo and Ebbesmeyer (1976) to determine the intensity of such processes from the simulated "drogue" velocities. Table 1 compares the mean values of γ, η, α, and h estimated for experiments ST and NST. The magnitudes of the vorticity, stretching, and shearing deformation rates are considerably increased under stratified conditions relative to the non-stratified case, leading to higher dispersion rates. Also the divergence rate γ is less negative, revealing the effect of baroclinic pumping creating divergence of the surface currents at the eastern end of the Oaks Arm after the diurnal wind events. The higher shearing deformation is also the result of baroclinic pumping, which concentrates the return westward flow along the north shore in the early morning hours, creating significant horizontal shear.

TABLE 1. Horizontal divergence (γ), relative vorticity (η), stretching (α), and shearing deformation (h) in the non-stratifying experiment (NST) and the stratifying experiment (ST), calculated following Okubo and Ebbesmeyer (1976).

Parameter	NST	ST
γ	−9.46	−2.58
η	3.96	31.4
α	2.19	17.7
h	6.84	21.5

Notes: For all parameters, units are $10^{-6}s^{-1}$. For the calculation of the mean shearing deformation, the absolute values of the individual hourly quantities were averaged. In all other cases, the signs of the values were considered.

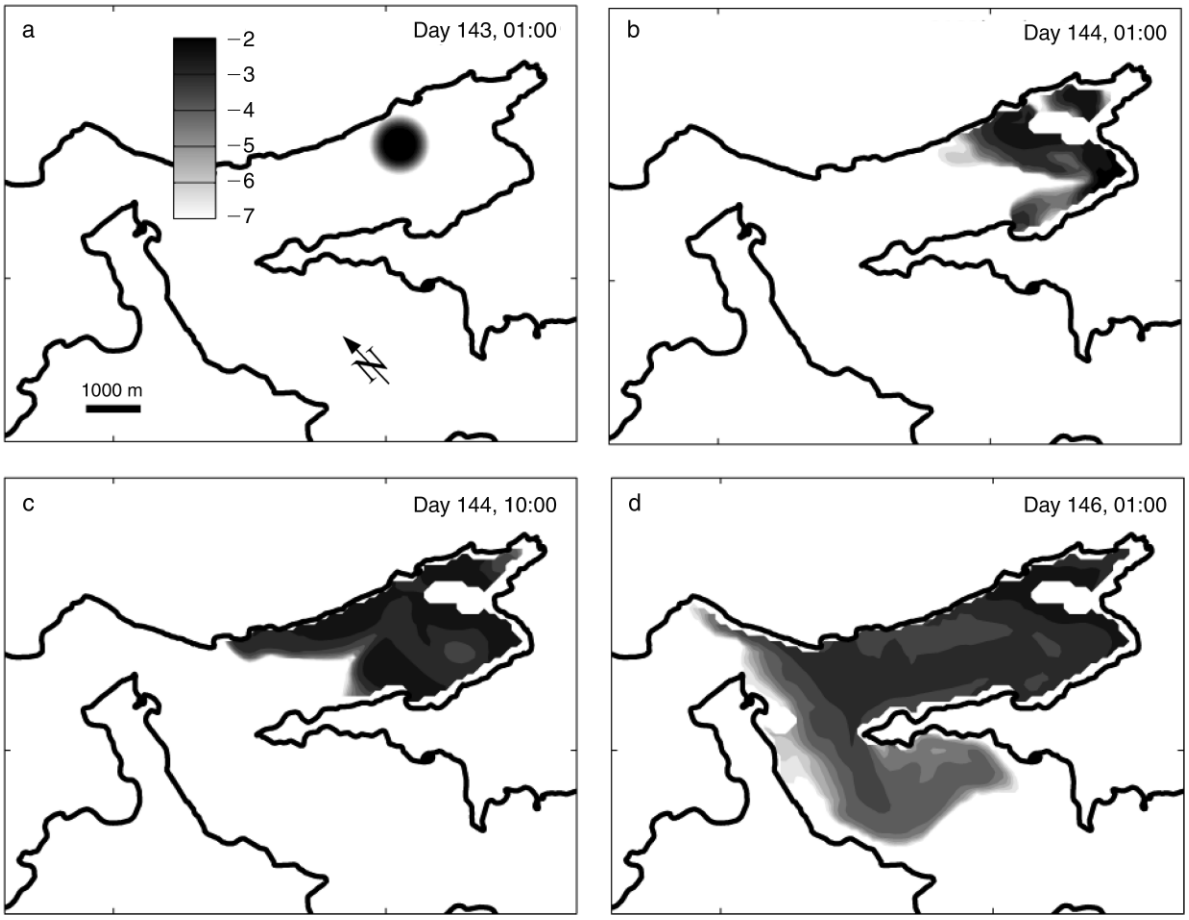

FIG. 11. Simulated tracer distribution 1.5 m below the surface (a) at release time, (b) 24 h after release, (c) 34 h after release, and (d) 72 h after the release of the tracer (in 1999), revealing the hydraulic connection of the Oaks Arm and the Lower Arm through surface currents. The gray scale shown in panel (a) represents values of the log (base 10) tracer concentration.

Migration paths to the upper and lower basins

Numerical tracer release experiments.—The advection-diffusion equation for tracer plumes represents the behavior of an ensemble of particles being carried by currents and diffused by turbulent processes, i.e., its solution is equivalent to repeating a large number of times the tracking exercise presented in the last section. In this section the solution of the transport equation is presented for a passive dissolved tracer released in two locations in the Oaks Arm; this solution confirms some of the phenomena described for the Oaks Arm in Rueda and Schladow (2003). In these simulations the tracer was only advected by the mean lake currents.

The initial concentration is that of a Gaussian cloud with the center of mass at 1.5 m depth and at the horizontal location shown in Fig. 11a. Fig. 11a–d shows the log (base 10) of the tracer concentration 1.5 m below the surface at the release time (day 143 at 01:00) and at three later times. The concentrations are normalized with the centerline concentration of the initial cloud. Twenty-four hours after the release (Fig. 11b) the tracer plume has been deformed, and some of it has been transported by wind-driven surface currents to the southeast end of the Oaks Arm. Nine hours later (Fig. 11c) the tracer is pushed back to the west along the north shore, following the baroclinicly generated return currents. This illustrates quite remarkably the setup and relaxation of temperature gradients influenced by the Earth's rotation, or baroclinic pumping (Rueda and Schladow 2003, Rueda et al. 2003). Seventy-two hours after the release (Fig. 11d), the tracer has entered the Lower Arm and starts to move south following the north shore of that arm.

Fig. 12a–d displays the concentration field 6.5 m below the water surface at the same times. The cloud is released near the lake surface at the location shown in Fig. 11a, and thus the concentration of the tracer is initially zero at 6.5 m (Fig. 12a). The tracer then plunges to this depth as a result of the action of the wind-driven downwelling currents at the easternmost end of the Oaks Arm (Fig. 12b). Nine hours later the tracer is pushed back to the west, mainly following the north shore (Fig. 12c), and after three days (Fig. 12d), the tracer at 6.5 m has entered the Upper Arm.

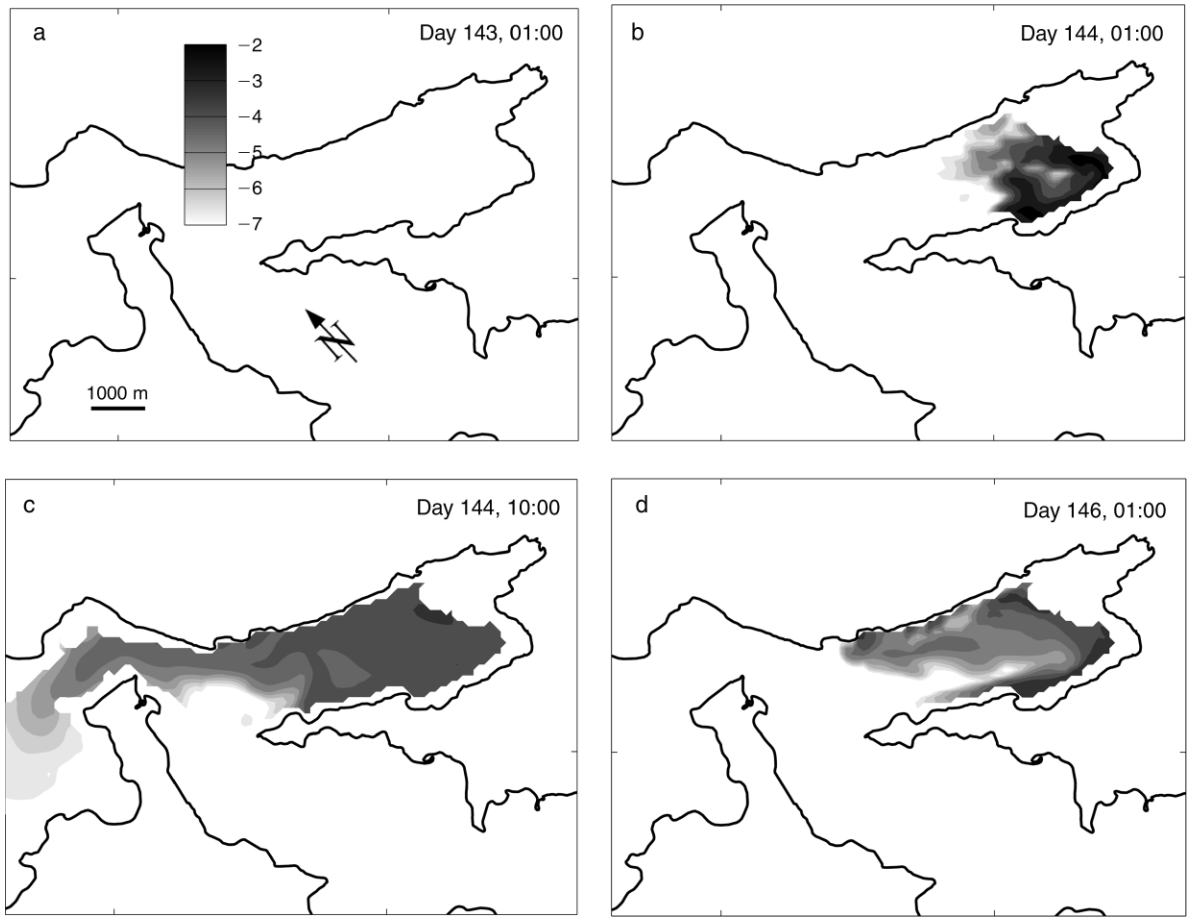

FIG. 12. Simulated tracer distribution 6.5 m below the surface (a) at release time, (b) 24 h after release, (c) 34 h after release, and (d) 72 h after the release of the tracer (in 1999), revealing the hydraulic connection with the Upper Arm in the lower layers. The gray scale shown in panel (a) represents values of the log (base 10) tracer concentration.

Mechanisms of inter-basin exchange

Figs. 11d and 12d evidence two very characteristic features of the exchange between the three basins of Clear Lake. First, inter-basin exchange is greatly accelerated when the lake exhibits thermal stratification. Second, contaminants originating in the Oaks Arm will reach the Lower Arm mainly by transport with the surface currents, while they will enter the Upper Arm by transport with the deeper currents. This decoupling of the surface and bottom transport was evident during the SF_6 tracer experiment. The numerical results can be used to understand the mechanism that drives this phenomenon.

Consider first the direct action of the wind on the stratified water columns of the three basins of Clear Lake. The northwesterly wind will carry surface water downwind (toward the easternmost ends of all three basins) and displace bottom water upwind (toward the westernmost ends). This vertical distribution of currents also occurs at the Narrows, in response to wind. If the lake were homogeneous, this circulation would weaken and eventually vanish by frictional effects after the forcing wind ceased. The spin-down time, T_{spin}, can be estimated from simple dimensional arguments applied to a simplified balance between the unsteady and the vertical diffusion terms in the longitudinal momentum equation, which gives

$$T_{\text{spin}} = \frac{H^2}{K_V}. \tag{11}$$

Here H is the depth of the water column and K_V is the vertical diffusivity. Using $H \sim 10$ m and $K_V \sim 0.01$ m/s^2 gives a spin-down time of ~3–4 h.

Under stratified conditions, the horizontal temperature gradients set up within each basin will drive baroclinic currents, long after the wind has ceased and in the opposite direction to the wind-driven current. This was demonstrated in the previous sections. In addition, the major constriction that occurs at the Narrows will allow the formation of a horizontal temperature gradient between the downwind end of the Upper Arm and the upwind ends of the Oaks and Lower Arms. Warmer water from the surface layers in the Upper Arm will accumulate to the west of the Narrows, and colder

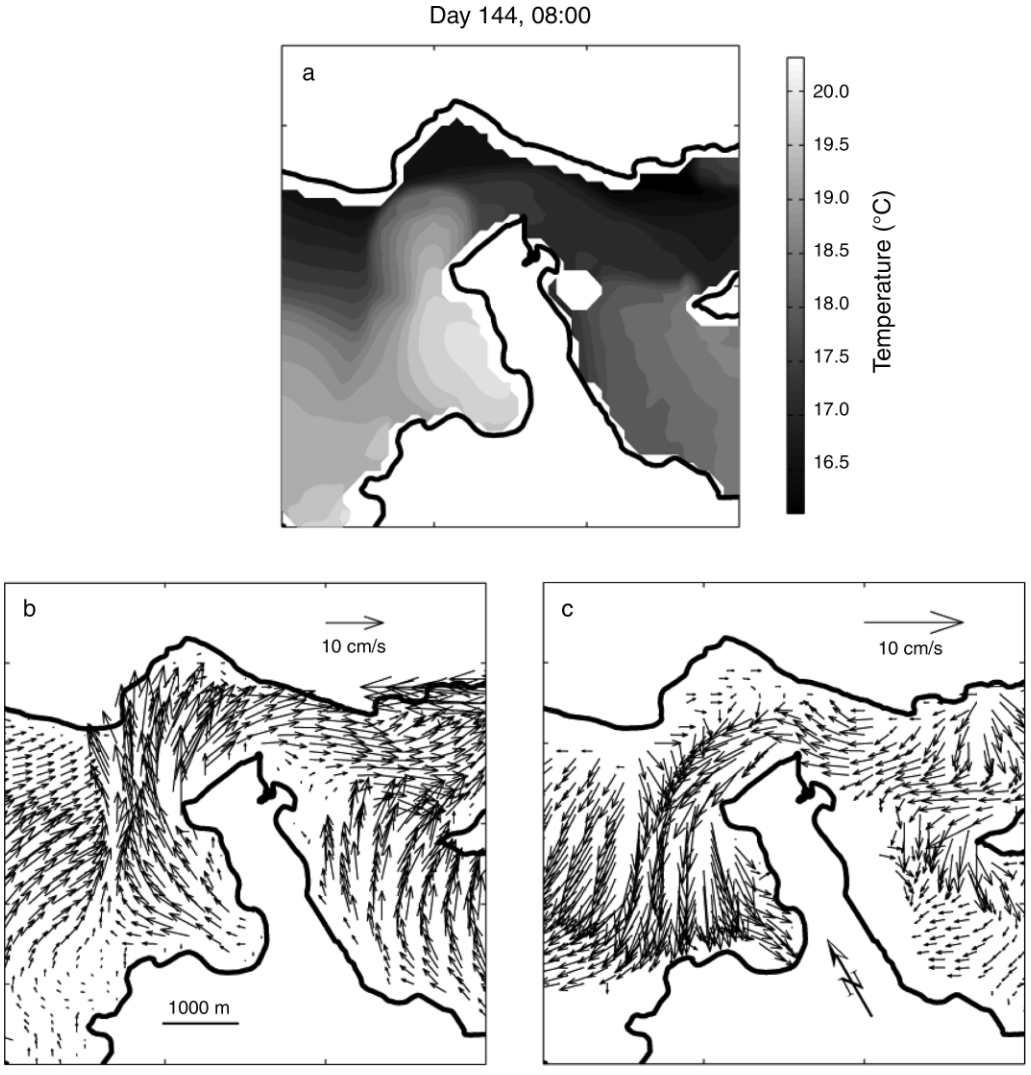

FIG. 13. Simulated temperature and velocity fields at 08:00 on day 144 (in 1999), in the vicinity of the Narrows. (a) Simulated temperature field 1 m below the surface; (b) simulated velocity field 1 m below the surface; and (c) simulated velocity field 8 m below the free surface. The scales of the arrows are shown in the upper right corner of panels (b) and (c).

water will accumulate at the upwind ends of the Lower and the Oaks Arms (see Fig. 13). This distribution of temperatures will force, under calm conditions, a baroclinicly driven exchange between the basins that has the same character as the direct wind-driven exchange. In this manner the inter-basin exchange is extended until the next wind event, and there is a flow of surface water, first from the Upper Arm through the Narrows to the west end of the Oaks Arm and then southward into the Lower Arm, carrying some proportion of Oaks Arm contaminants. At the same time, there is a flow of bottom water from the Oaks Arm through the Narrows into the Upper Arm.

CONCLUSIONS

A series of tracer experiments and numerical model runs have been conducted to characterize the mechanisms of transport and dispersion of water and particles in Clear Lake, a large multi-basin and polymictic lake in northern California. Even though the numerical modeling and the field experiments do not correspond to the same periods, the main conclusions from both were very consistent. Conclusions, based solely on the tracer experiments, provided new information on contaminant transport in this system. Under stratified conditions, the rate of spreading of the tracer was large. In one case the fluorescent tracer was "lost" because of the rapidity of the advective flows, whereas in another case a gaseous tracer was seen to move throughout the basins within days of release. The tracer developed a very patchy distribution due to slow mixing and loss from the lake via gas exchange with the atmosphere. In less than one week it had spread from the eastern end of the Oaks Arm to the other basins, the precise timing being

unknown due to the low sampling frequency. Under non-stratified conditions, the tracer spread more slowly and had a concentration that gradually diminished with distance from the injection location.

Using the numerical results, the mechanisms accounting for these observed patterns can be understood. The results reveal that transport in this, and probably most large polymictic lakes, occurs in pulses, with maximum rates coinciding with the stratified periods. Stratification acts first to enhance the currents by inhibiting vertical momentum mixing and decoupling the surface currents from bottom friction. Stratification also favors horizontal dispersion processes. The multitude of flow structures (such as horizontal gyres and fronts) that result from the interaction of the wind and the density fields in the lake is responsible for such higher dispersion rates. The inter-basin exchange patterns and the forcing mechanisms were examined with the aid of numerical tracer experiments and the results from the 3-D hydrodynamic model. Any contaminants originating in the Oaks Arm would penetrate into the Lower Arm following the surface currents or into the Upper Arm mainly through the bottom currents. It was shown that, under stratified conditions, the baroclinic (density-driven) gradients and the wind forcing act jointly to exacerbate the inter-basin exchange. The density differences created along the Narrows prolong the period of active exchange beyond the duration of the diurnal wind events and account for the vertical separation of the flows out of the Oaks Arm.

Acknowledgments

Peter Smith provided invaluable help with the numerical model, and Stephen Monismith and Mark Stacey collaborated on related parts of the experimental program. We are indebted to graduate students in the Environmental Dynamics Laboratory (EDL), who assisted in the instrument deployment and retrieval; in particular we thank Michelle Lynch, John Warner, Brian Heiland, Bill Fleenor, Sveinn Palmarsson, and George Croll. Laura Rademacher of UCSB assisted with the SF_6 sampling and analysis. The authors wish to thank the staff of the Clear Lake Environmental Research Center, Clear Lake Air Quality Management District, and Norman and Porter Anderson of Vector Control for their assistance. This work was partially supported by the Spanish Ministry of Education and Science, the U.S. EPA (R819658 and R825433) Center for Ecological Health Research at UC Davis, U.S. EPA (GR825428-01-0) Science to Achieve Results (STAR) program, and the U.C. Toxic Substances Research and Teaching Program. Although the information in this document has been funded in part by the U.S. Environmental Protection Agency, it may not necessarily reflect the views of the Agency and no official endorsement should be inferred.

Literature Cited

Bullister, J. L., D. P. Wisegarver, and R. E. Sonnerup. 2006. Sulfur hexafluoride as a transient tracer in the North Pacific Ocean. Geophysical Research Letters 33:L18603. [doi: 10.1029/2006GL026514]

Busenberg, E., and L. N. Plummer. 2000. Dating young groundwater with sulfur hexafluoride: natural and anthropogenic sources of sulfur hexafluoride. Water Resources Research 36:3011–3030.

Chamberlin, C. E., R. Chaney, G. Finney, M. Hood, P. Lehman, M. McKee, and R. Willis. 1990. Abatement and control study: Sulfur Bank Mine and Clear Lake. Environmental Resources Engineering Department, Humboldt State University, Arcata, California, USA.

Clark, J. F., G. B. Hudson, M. L. Davisson, G. Woodside, and R. Herndon. 2004. Geochemical imaging of flow near an artificial recharge facility, Orange County, CA. Ground Water 42:167–174.

Clark, J. F., P. Schlosser, M. Stute, and H. J. Simpson. 1996. SF_6-^{3}He tracer release experiment: a new method of determining longitudinal dispersion coefficients in large rivers. Environmental Science and Technology 30:1527–1532.

Clark, J. F., R. Wanninkhof, P. Schlosser, and H. J. Simpson. 1994. Gas exchange in the tidal Hudson River using a dual tracer technique. Tellus 46B:274–285.

Dimou, K. N., and E. E. Adams. 1993. A random-walk, particle tracking model for well-mixed estuaries and coastal waters. Estuarine, Coastal and Shelf Science 37:99–110.

Dunsbergen, D. W., and G. S. Stelling. 1993. A 3-D particle model for transport problems in transformed coordinates. Publication number 93-7. Delft University of Technology. Department of Civil Engineering, Hydraulic and Geotechnical Engineering Division, Hydromechanics Group, Delft, The Netherlands.

Fischer, H. B., E. J. List, R. C. Y. Koh, J. Imberger, and N. H. Brooks. 1979. Mixing in inland and coastal waters. Academic Press, New York, New York, USA.

Gamlin, J. D., J. F. Clark, G. Woodside, and R. Herndon. 2001. Large-scale tracing of ground water with sulfur hexafluoride. ASCE Journal of Environmental Engineering 127:171–174.

Halide, H., and B. G. Sanderson. 1993. Determining flow field singularities from drifter trajectories. Journal of Geophysical Research 98(C5):8413–8423.

Kantha, L. H., and C. A. Clayson. 1994. An improved mixed layer model for geophysical applications. Journal of Geophysical Research 99(C12):25235–25266.

Kitanidis, P. K. 1994. Particle-tracking equations for the solution of the advection-dispersion equation with variable coefficients. Water Resources Research 30:3225–3227.

Knauer, K., H. M. Nepf, and H. F. Hemond. 2000. The production of chemical heterogeneity in Upper Mystic Lake. Limnology and Oceanography 45:1647–1654.

Lawrence, G. A., K. I. Ashley, N. Yonemitsu, and J. R. Ellis. 1995. Natural dispersion in a small lake. Limnology and Oceanography 40:1519–1526.

List, E. J., G. Gartrell, and C. D. Winant. 1990. Diffusion and dispersion in coastal waters. ASCE Journal of Hydraulic Engineering 116:1158–1179.

Lynch, M. G. 1996. Seasonal variations in lake mixing, Clear Lake, California. Thesis. University of California, Davis, California, USA.

Okubo, A., and C. C. Ebbesmeyer. 1976. Determination of vorticity, divergence, and deformation rates from analysis of drogue observations. Deep-Sea Research 23:349–352.

Oton, S. M., S. G. Schladow, J. F. Clark, B. Hudson, and A. Dvorak. 1998. Hydrological transport between the Sulphur Bank Mercury Mine and Clear Lake using gas tracer. Pages 119–124 *in* Second Annual Clear Lake Science and Management Symposium, Lakeport, California. University of California, Davis, California, USA.

Pollock, D. W. 1988. Semianalytical computation of path lines for finite difference models. Groundwater 26:743–750.

Ramaswami, A., J. B. Milford, and M. J. Small. 2005. Integrated environmental modeling: pollutant transport, fate, and risk in the environment. John Wiley and Sons, New York, New York, USA.

Rueda, F. J. 2001. A three-dimensional hydrodynamic and transport model for lake environments. Dissertation. University of California, Davis, California, USA.

Rueda, F. J., and S. G. Schladow. 2002. Quantitative comparison of models for barotropic response of homoge-

neous basins. ASCE Journal of Hydraulic Engineering 128: 201–213.

Rueda, F. J., and S. G. Schladow. 2003. The internal dynamics of a large polymictic lake. Part II: three-dimensional numerical simulations. ASCE Journal of Hydraulic Engineering 129:92–101.

Rueda, F. J., S. G. Schladow, S. G. Monismith, and M. T. Stacey. 2003. The internal dynamics of a large polymictic lake. Part I: field experiments. ASCE Journal of Hydraulic Engineering 129:82–91.

Rueda, F. J., S. G. Schladow, S. G. Monismith, and M. T. Stacey. 2005. On the effects of topography on wind and the generation of currents in a large multi-basin lake. Hydrobiologia 532:139–151.

Schladow, S. G., and J. F. Clark. 2008. Use of tracers to quantify subsurface flow through a mining pit. Ecological Applications 18(Supplement):A55–A71.

Smith, P. E. 1997. A three-dimensional, finite-difference model for estuarine circulation. Dissertation. University of California, Davis, California, USA.

Suchanek, T. H., L. H. Mullen, B. H. Lamphere, P. J. Richerson, C. E. Woodmansee, D. G. Slotton, E. J. Harner, and L. A. Woodward. 1998. Redistribution of mercury from contaminated lake sediments of Clear Lake, California. Water, Air and Soil Pollution 104:77–102.

Suchanek, T. H., et al. 2008. The legacy of mercury cycling from mining sources in an aquatic ecosystem: from ore to organism. Ecological Applications 18(Supplement):A12–A28.

Wanninkhof, R., J. R. Ledwell, and W. S. Broecker. 1985. Gas exchange-wind speed relationship measured with sulfur hexafluoride on a lake. Science 227:1224–1226.

Wanninkhof, R., J. R. Ledwell, W. S. Broecker, and M. Hamilton. 1987. Gas exchange on Mono Lake and Crowley Lake, California. Journal of Geophysical Research 92:14567–14580.

PLATE 1. A photograph from an early postcard showing the Sulphur Bank Mercury Mine site ca. 1890 (courtesy of Lakeport Historic Courthouse Museum). The large complex of buildings at center right indicates the location of one of many shafts, which were active from ca. 1875 to 1902.

PLATE 2. Mercury-laden mine tailings and waste rock piles at the Sulphur Bank Mercury Mine ca. 1900, before more modern earthmoving equipment and bulldozing occurred (courtesy of Lakeport Historic Courthouse Museum).